Towards high-dimensional multiconfiguration time-dependent Hartree simulations of correlated electrons in the interparticle Coulombic decay process

Sara Marando,[1,2] Frederic Schubert,[1,2] Subhra K. Das,[3] Ramiro Salvai,[4] Daniel Peláez,[3,a)] and Annika Bande[1,4,b)]

[1)]*Helmholtz-Zentrum Berlin für Materialien und Energie, Hahn-Meitner-Platz 1, 14109 Berlin, Germany*

[2)]*Institute of Chemistry and Biochemistry, Freie Universität Berlin, Arnimallee 22, 14195 Berlin, Germany*

[3)]*Université Paris-Saclay, CNRS, Institut des Sciences Moléculaires d'Orsay, 91405, Orsay, France.*

[4)]*Institute of Inorganic Chemistry, Leibniz University Hannover, Callinstr. 9, 30167 Hannover, Germany*

(Dated: 21 November 2026)

The inter-quantum dot Coulombic decay is an efficient decay process in quantum dot dimers. However, to present, the respective electron dynamics simulations undertaken with the multiconfiguration time-dependent Hartree (MCTDH) method were limited to quantum dot dimers in nanowires or obtained from epitaxial growth, where the emitted electron is confined in one or two dimensions, because of the computational effort in evaluating the Coulomb interaction integral. In this letter we compare the already previously used multi-grid potfit with the Monte Carlo canonical polyadic decomposition (MCCPD) potential representation, which was recently shown to significantly accelerate high-dimensional MCTDH calculations. The MCCPD-based calculations are using a non-intuitive, coordinate-based mode combination of the two-electron system, which was found to be equally accurate as the particle-based mode combination. This study therefore serves as a benchmark paving the way to simulating ICD in colloidal quantum dot dimers with a three-dimensional continuum.

The interparticle Coulombic decay (ICD) is a non-radiative decay process of a delocalized resonance state involving two or more spatially separated species. It is driven by the long-range Coulomb interaction between electrons localized on the distinct system components. An electron in an excited energy level within one species undergoes a local relaxation, and the corresponding energy is non-radiatively transferred to the neighboring system, which is simultaneously ionized.[1–4] ICD takes place on a short timescale, ranging from a few femtoseconds in atomic and molecular systems to several picoseconds in nanostructures. In both cases, it outpaces comparable radiative decay channels by several orders of magnitude[4].

Several theoretical investigations on ICD have been performed in the time domain, employing the multiconfiguration time-dependent Hartree (MCTDH) method.[5–8] These calculations addressed semiconductor quantum dot (QD) dimers described by a binding potential model with two active electrons. Since the resonance states possess a bound-like character with a finite coupling to the continuum, the MCTDH approach provides an efficient and accurate framework via its flexible multiconfiguration wave function in the basis of time-dependent orbitals and the underlying discrete variable representation (DVR) treating bound and continuum states on the same footing.[9–11] Most of the studies have relied on a quantum dot model with only a single continuum dimension, which enables a computationally tractable representation in the necessarily large DVR basis in that dimension.[7,8,12–14] Beyond the issues regarding the continuum, a second computational bottleneck is the representation of the Coulomb interaction potential. In its full form, it is a six-dimensional potential and does not admit a low-rank sum-of-products factorization.[13] In a simple one-dimensional model, this challenge is mitigated by employing either an effective two-dimensional Coulomb term[8] or by treating the bound dimensions with a very small harmonic oscillator basis.[5,14]

To cover a wider range of technically possible QD systems, a two-dimensional (2D) model system was set up.[13] In the case of two electrons and an effective Coulomb interaction term, the 2D model maps onto a four-dimensional configuration space. As stated before, describing both bound and continuum states implies that the primitive grid should have wide boundaries and a high density of grid-points. Moreover, MCTDH requires all operators to be in separable form.[9] To bring the potential (a local operator) in such form, one uses tensor decomposition methods. Unfortunately, commonly employed approaches (e.g. POTFIT[15]) relying on the Tucker form (see Eq.6) severely struggle with dimensionality and high grid densities. This was partially overcome by the variational multigrid POTFIT (MGPF) method.[16] In MGPF, one avoids the computation of the (far too large) primitive grid in full. Instead, the computation of core tensor and factor matrices is performed in a series of nested grids. We employed this strategy in a previous study to analyze the decay rates of two resonances as a function of the inter-dot distance.[13] The MGPF potential allowed even the extension toward a system with three electrons in three QDs.[12] However, extending the QD model towards a three dimensional continuum, as it would be needed to simulate colloidal QDs emitting the ICD electron

[a)]Electronic mail: daniel.pelaez-ruiz@universite-paris-saclay.fr

[b)]Electronic mail: annika.bande@aci.uni-hannover.de

to all spatial directions, remains computationally unfeasible.

This work paves the path towards such a goal. It introduces the use of the canonical polyadic decomposition (CPD) method fully compatible with MCTDH. On top of that, the usual electronic wavefunction (and the associated potential) is re-expressed in terms of coordinates which decouple the physical particles. This numerical strategy is expected to lead to a very compact CPD representation and concomitantly to very efficient MCTDH simulations. These numerical procedures are applied to the study of ICD processes in a well-investigated QD dimer model with a two-dimensional continuum. Its validity is assessed by comparison with MGPF results.

The targeted two-electron system is a previously studied dimer of quasi two-dimensional QDs that have each a two-dimensional continuum in the x and z directions, while the third dimension is neglected as it is not of relevance to the ICD process.[13] The electronic Hamiltonian in atomic units is given by

$$\hat{H}_{\mathrm{el}} = \sum_{i=1}^{2} \Big[-\frac{1}{2}\frac{\partial^2}{\partial x_i^2} - \frac{1}{2}\frac{\partial^2}{\partial z_i^2} + \hat{V}^{\mathrm{QD}}(x_i, z_i) \Big] + \hat{V}^{\mathrm{rC}}(x_1, x_2, z_1, z_2) + \hat{V}^{\mathrm{CAP}}. \tag{1}$$

Its first term is the kinetic energy associated with the four electronic coordinates. The confinement potential imposed by the quantum dots on each electron reads

$$V^{\mathrm{QD}}(\hat{x}, \hat{z}) = -D \sum_{j=L,R} \exp\left\{ -b_j \left[(\hat{z} - z_j)^2 + \hat{x}^2 \right] \right\} . \tag{2}$$

The model consists of a sum of negative Gaussian potentials of depths D and widths $r_{L,R}$ parametrized in $b_{L,R} = 4\ln(2)/r_{L,R}^2$, which are aligned along the z axis and located at positions $\pm z_j$.

The ICD process is mediated by the Coulomb interaction,

$$\hat{V}^{\mathrm{rC}}(r_{12}) = \left(r_{12}^2 + a^2 e^{-b r_{12}} \right)^{-1/2}, \tag{3}$$

which contains the distance between the 2D electrons,

$$r_{12} = |\vec{r}_1 - \vec{r}_2| = \sqrt{(x_1 - x_2)^2 + (z_1 - z_2)^2}\,.$$

To eliminate the ICD continuum electron that would otherwise be reflected at the grid boundaries, complex absorbing potentials are applied in both directions of each degree of freedom, $q_i = x_1, x_2, z_1, z_2$, defined as[17–19]

$$\hat{V}^{\mathrm{CAP}} = \sum_{q_i} -i\eta \Big[(q_i - q_{\mathrm{CAP}})^4 \, \Theta(q_i - q_{\mathrm{CAP}}) + (q_i + q_{\mathrm{CAP}})^4 \, \Theta(-q_i - q_{\mathrm{CAP}}) \Big] . \tag{4}$$

η is the CAP strength and Θ is the Heaviside step function. The fourth-order CAPs start acting at a distance q_{CAP} from the origin, which is chosen sufficiently far from the quantum dot region to avoid interaction with the bound part of the wavefunction.

The MCTDH method is employed for solving the time-dependent Schrödinger equation. Here, the total wavefunction is represented as a sum of Hartree products of time-dependent single-particle functions (SPFs), each weighted by a time-dependent coefficient. For a two-electron system with two spatial degrees of freedom per electron, the wavefunction is expressed as

$$\Psi(x_1, x_2, z_1, z_2, t) = \sum_{j_1=1}^{n_1} \sum_{j_2=1}^{n_2} A_{j_1 j_2}(t) \, \varphi_{j_1}^{(1)}(x_1, x_2, t) \, \varphi_{j_2}^{(2)}(z_1, z_2, t), \tag{5}$$

where the coordinates of the two electrons are grouped together in the SPFs $\varphi_{j_1}^{(1)}(x_1, x_2)$ and $\varphi_{j_2}^{(2)}(z_1, z_2)$ in a recently developed coordinate-based mode combination (cb).[20] This stands in contrast to the previous, more intuitive, particle-based mode combination (pb), in which each electron is represented by a given set of SPFs (i.e. $\varphi_{j_1}^{(1)}(x_1, z_1)$ and $\varphi_{j_2}^{(2)}(x_2, z_2)$). It should be noted that antisymmetrization in the pb scheme is straightforward[5,13,21], however the CPD potential representation turns out to be more favorable using the cb scheme. This will be further discussed in a subsequent work.

All objects in an MCTDH simulation, such as the potential energy surfaces, are represented in a separable form. This allows for an efficient evaluation of multidimensional matrix elements while, at the same time, enables their compression.[9] To achieve this tensor decomposition methods are utilized. These are characterized by an ansatz and, the most common ones, utilize a Tucker (Eq. 6) or a canonical polyadic (CP, Eq. 7) ansätze. Two of these methods, POTFIT[15], and MGPF[16], share the same Tucker functional form

$$V_{i_1,\ldots,i_f}^{\mathrm{Tucker}} = \sum_{j_1=1}^{m_1} \cdots \sum_{j_f=1}^{m_f} C_{j_1 \ldots j_f} \prod_{\kappa=1}^{f} v_{i_\kappa, j_\kappa}^{(\kappa)}. \tag{6}$$

where f denotes the number of degrees of freedom, m_κ is the number of basis functions for the κ-th mode, $v^{(\kappa)}$ a factor matrix, and $C_{j_1,\ldots,j_f}$ is an entry of the the core tensor. As it can be observed, the number configurations ($\prod_{\kappa=1}^{f} v_{i_\kappa, j_\kappa}^{(\kappa)}$) grows exponentially with the number of dimensions. In contrast to this exponential scaling of Tucker, the so-called canonical polyadic decomposition ansatz,

$$V_{i_1,\ldots,i_f}^{CP} = \sum_{r=1}^{R} \lambda_r \prod_{\kappa=1}^{f} v_{i_\kappa, r}^{(\kappa)} , \tag{7}$$

is separable and scales linearly. In this expression, the sum runs up to R configurations, weighted by λ coefficients (cf. with the C tensor in Eq. 6). As it can be readily noticed, the CP is much more compact than the Tucker representation. This remarkable combination of low rank and high accuracy can be attributed to the non-orthogonality of the CP basis. These advantages of CP over Tucker have been dramatically enhanced in the so-called Monte Carlo CPD (MC-CPD) in which the integrals needed in the CPD process have been replaced by the stochastic counterparts.[22] This promises for some profit for this work, showing that CP is able to

produce compact Coulomb representations of high accuracy. These will enable electron dynamics simulations on grids much denser than the ones attainable by using Tucker-based methods. It should be noted that, for the sake of consistency, the MCCPD representation is benchmarked against MGPF.

MCTDH calculations are executed using the Heidelberg program in its version 8.6.7.[23,24] The parametrization was adapted from previous work to ensure both comparability of results and a meaningful description of self-assembled GaAs QDs.[13] The original calculations of 2019 in a particle-based mode combination using the MGPF potential were repeated using the current MCTDH version, allowing thus to verify the reproducibility of the original results and a valid comparison. New calculations are using the coordinate-based modes in conjunction with the MCCPD potential.

All calculations were carried out in atomic units. For the sake of readability and to enable direct comparison, the physical quantities have been converted into the material-specific international system (SI) units of GaAs using the effective mass approximation.[8,25] In this framework, an effective electron mass of $m^* = 0.063$ and a dielectric constant of $\varepsilon = 12.9$ were employed.[26]

The two Gaussian-shaped potentials have both the identical depths of $D = 21.67$ meV. $r_L = 36.08$ nm and $r_R = 18.04$ nm where $r_{L,R}$ correspond to the lateral diameters of the left and right QD, respectively. The wavefunctions and operators are represented on a sine DVR with 140 grid points within the interval $[-54.18\text{ nm}, 54.18\text{ nm}]$.

In order to simulate the ICD process in a time-dependent frame, one has to determine the two-electron resonance states of the QD model system which will be taken as the initial states. To this end, a block-improved block relaxation is carried out, i.e. a propagation in negative imaginary time.[27] It optimizes several eigenstates simultaneously. Here, the lowest 10 states are converged above an energy slightly below that of the expected state given with `rlemin` command. $n_k = 20$ SPFs per mode were optimized iteratively by relaxation using the 8$^{\text{th}}$-order Runge-Kutta scheme with an error tolerance of 10^{-9} a.u. and initial step size of 1.0 a.u., while the A-coefficients are computed by diagonalization with the Davidson algorithm. This allows for a faster convergence than a standard relaxation procedure.[28] A constant mean field (CMF) integrator is applied, with a numerical accuracy of 10^{-2} a.u. for the relaxation step. The CMF step size is fixed to 0.2 a.u. in all calculations. While in the pb mode combination, antisymmetrization is straightforwardly achieved by imposing the condition $A_{j_1 j_2}(t) = -A_{j_2 j_1}(t)$ onto the A vector to work with a triplet state, the algorithm was extended to enforce a desired exchange symmetry at each iteration step in the cb mode combination.[20] Finally, the resonances are identified numerically by their energy and visually by the electron density. The latter is obtained by integrating over the coordinates of the second electron, $\rho(x,z,t) = \rho(x_1,z_1,t) = \iint |\Psi(x_1,x_2,z_1,z_2,t)|^2\, dx_2\, dz_2$, in the case of the initial state using the time-independent wave function.

The decay behavior of the resonances RES-X and RES-Z is obtained by starting a time propagation using the respective resonance as initial state. Here, $n_k = 12$ SPFs are used.

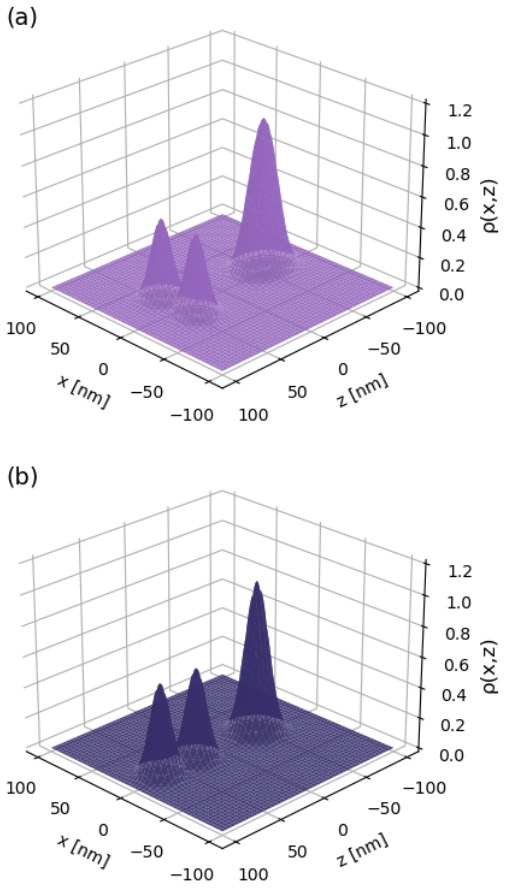


FIG. 1: Two-electron densities of the resonance states (a) RES-X and (b) RES-Z.

The CMF integrator accuracy is set to 10^{-7} a.u., the Runge–Kutta error tolerance to 10^{-7} a.u., and the initial step size to 1.0 a.u. The time evolution is carried out using the short iterative Lanczos algorithm, well suited for large matrix systems. The method is implemented with an order of 15 and a time step of 10^{-7} a.u. The total propagation time amounts 1.0×10^4. During propagations, the permutation symmetry operator is conserved. Therefore, the standard MCTDH propagation scheme is employed, ensuring the preservation of symmetry through an appropriately defined initial wavefunction. The CAP is exclusively used in propagations. Its strength is set to $\eta = 8.70 \times 10^{-6}$ a.u. The absorbing regions begin at $q_{\text{CAP}} = 30$ nm from the center of the simulation grid. To obtain the rates, the absolute squared of the crosscorrelation function among the resonance state function and the time-dependent wave function is computed. It decays exponentially as the resonance becomes unpopulated and the exponential factor delivers the ICD rate.

To understand the form of the resonance states obtained as ICD decaying states, notion of the single-electron levels of the electronic structure is helpful.[13] It features three quantized single-electron levels along the x and four along the z direction. The herein relevant levels are X_m with $m = 0, 1$, which

are the lowest and the first excited levels of both QDs in the x direction as well as Z_n with $n = 0, 1, 2$. The first and third states are the ground and first excited levels of the left QD, while the second state is the lowest level of the right QD. These levels yield three two-electron product states $|X_m Z_n\rangle$ relevant to ICD, which can be deduced from relaxation calculations. Their densities are displayed in Fig. 1. The ground state (GS), $|X_0Z_0, X_0Z_1\rangle$, has one electron in the lowest level of the left QD ($|X_0Z_0\rangle$) and another in the lowest level of the right QD ($|X_0Z_1\rangle$). The lower-energy resonance in the x-direction (RES-X), $|X_1Z_0, X_0Z_1\rangle$ has the electron in the left QD excited to the first level in x, the higher-energy (RES-Z), $|X_0Z_2, X_0Z_1\rangle$ has the same QD excited into the first level in the z direction, while in both cases the other electron remains placed as in the GS.

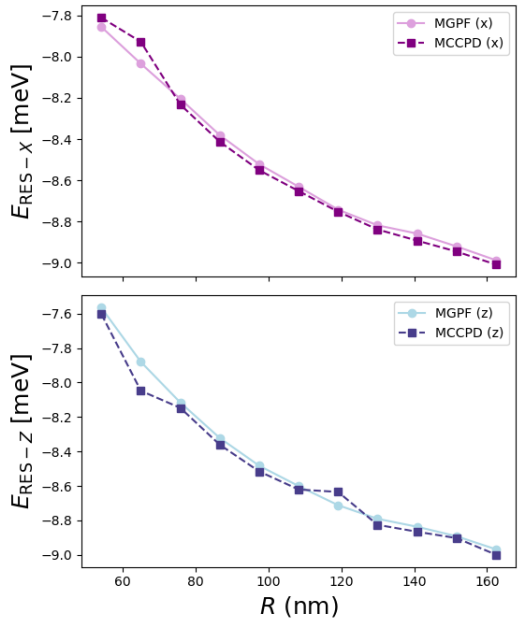


FIG. 2: Comparison between the energies of the resonances, (a) RES-X and (b) RES-Z, using MGPF and MCCPD in meV as a function of the interdot distance R (nm).

The energies of RES-X and RES-Z are displayed in Fig. 2. Across the entire range of separations and with either method, the resonance energies become more negative as R increases, indicating a stabilization of the resonance state with decreasing Coulomb interaction as the dots move further apart, as was observed in many previous ICD studies and numerically identical in Ref.[13].

For both resonances, MCCPD energies are generally by only below 0.05 meV (0.40%) more negative than MGPF throughout the range with two outliers at $R = 66.09$ nm and 119.13 nm. At these critical interdot distances (more so at $R = 64.98$ nm, not shown) the resonance approaches the continuum threshold and the quasi-bound character of the state weakens. As a result, neither does the density show clearly only the form of that of a resonance, nor is the energy exclusively applying to the resonance. For RES-X at the shortest distances, the MCCPD energy is less negative. Here, an overlap of the two electrons' orbitals is not fully excluded, i.e. one is not in the asymptotic regime, which may result in a different behavior with the two different methods.

Nonetheless, the MCCPD results very closely follow the MGPF values over the full range, confirming the consistency between the two methods. Thus, for relaxation calculations it is possible to faithfully replace the computationally limited MGPF approach in conjunction with a pb basis by the more straightforward MCCPD method in a cb basis.

The wave functions RES-X and RES-Z obtained in the block-relaxation calculation are used as input states for the time-dependent simulations from which the ICD process can be triggered and monitored. The selection of these states allows for a direct comparison, while also enabling the investigation of the role of Coulomb coupling and potential representations (Tucker vs. CP) in the decay dynamics. In order to analyze the distance dependence of the ICD process, the decay rates Γ were computed for quantum dot separations in the range $R = 54.15$–162.45 nm. Their plot can be found in Fig. 3.

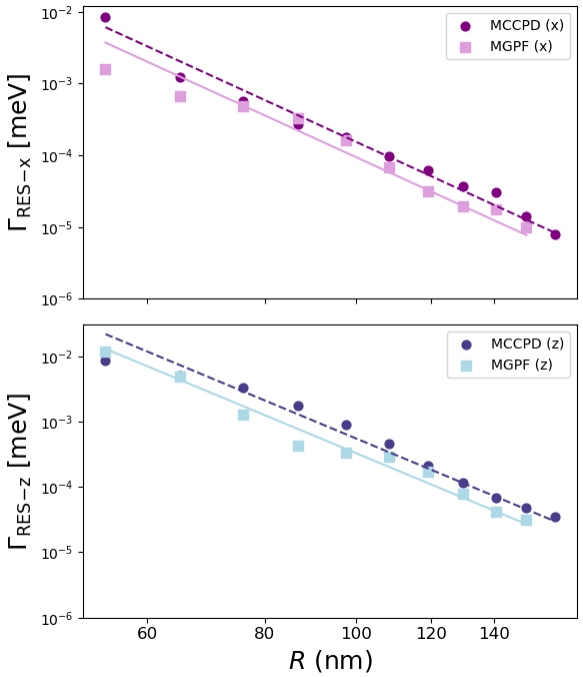


FIG. 3: Decay rates $\Gamma_{\text{RES-X}}$ and $\Gamma_{\text{RES-Z}}$ as a function of quantum dot separation R (nm), shown in a double logarithmic scale. The data points for the decay along the x direction are represented by circles around a solid fit line R^{-6}, while the decay along z is indicated by triangles around a dashed line.

The ICD decay rates $\Gamma_{\text{RES-X}}$ and $\Gamma_{\text{RES-Z}}$ show a clear decrease as the interdot separation R increases. The corresponding lifetimes $\tau_{\text{RES-X}}$ and $\tau_{\text{RES-Z}}$ increase accordingly: for instance for the MCCPD data, $\tau_{\text{RES-X}}$ grows from 7.69×10^1 ps at $R = 54.15$ nm to 1.05×10^4 ps at $R = 119.13$ nm, and further to 4.66×10^4 ps at $R = 151.62$ nm, i.e., tens of nanoseconds for the largest separations considered. The decay times of RES-Z are slightly smaller. Since the lifetimes are simply the inverse of the de-

cay rates, the small differences between $\tau_{\text{RES-X}}$ and $\tau_{\text{RES-Z}}$ translate into proportionally small differences between $\Gamma_{\text{RES-X}}$ and $\Gamma_{\text{RES-Z}}$.

Focusing on the rates in Fig. 3, one discrepancy among methods arises for small separations ($R = 54.15$ nm). Here, the MCCPD rates (points in both panels) along x and z are nearly identical, while they differ substantially with MGPF. In agreement to previous findings the rates at shortest distances are affected by the overlap of orbitals and do not follow the long-range behavior. For all larger R, all curves from the MCCPD and the MGPF ansatz display the general trend in which the rate decay is consistent with the long-range character of the dipole–dipole interaction, which follows an R^{-6} dependence,[29,30] as is also confirmed by the respective fits in Fig. 3.

As the distance increases, the two components remain of the same order of magnitude, with $\Gamma_{\text{RES-Z}}$ being larger than $\Gamma_{\text{RES-X}}$. This finding was explained earlier[13] based on the MGPF computations: The overlap of electrons in the resonance wave function $|X_0Z_2, X_0Z_1\rangle$ (RES-Z) is larger than the overlap in $|X_1Z_0, X_0Z_1\rangle$ (RES-X), as can be seen by visual inspection from Fig. 1. To this end, the Coulomb interaction is likewise larger and thus the rate, leading to a faster decay of RES-Z.

Another observation uniform to both approaches and known from earlier inspections is the following: The decay rates oscillate around the R^{-6} fit. This can be understood from the effective potential arising from the relaxing electron that hinders the emitted ICD electron to freely move in all directions, thus affecting the rate. In cases of a one-dimensional continuum this effect is very strong.[5,13] Here the oscillations in the MGPF framework display maximal (average) deviations of 50% (24%) for the decay of RES-Z and 58% (30%) for that of RES-X (which agrees with Ref.[13]), whereas the MCCPD calculations exhibit maximal (average) deviations of 61% (23%) for RES-Z and 54% (22%) for RES-X. As the shape of this effective barrier is neatly connected to the exact shape of the Coulomb potential over the whole coordinate, it is not possible to explain this effect only from the data, but in general both methods give an oscillation in the same order of magnitude.

Another difference among the methods is on the rate values: because the decay rates are extremely small, relative percentages artificially amplify the differences between CPD and MGPF, leading to values of order 140%, which is exceeding the oscillation discussed above, but still in the same order of magnitude. In absolute terms, however, the deviations remain tiny: the typical discrepancy is on the order of 10^{-3} meV, and the long-range R^{-6} behaviour differs by only $\sim 10^{-3}$ meV nm^6.

Despite the resonance state energies being slightly lower with MCCPD, the rates are higher. This is counterintuitive, as a larger Coulomb repulsion would facilitate ICD. However, the resonance energy is a global quantity that applies to the total system, while the Coulomb potential may have local differences that lead to this effect, which – as for the oscillations – may modify the rates in the dynamical simulation. It is to be noted, that the differences discussed here are tiny and do not affect the overall physics.

Conclusively, the present analysis provides a consistent and comprehensive picture of both the electronic structure and the ICD dynamics in a coupled QDs system. The comparison between the MGPF data reproduced in accord with Ref.[13] and the MCCPD results newly obtained in this work demonstrate that the two approaches exhibit the same physical trends with high fidelity. Although small numerical deviations are observed, these differences are not surprising given the numerical differences of these representations of the Coulomb operator.

From a physical perspective, one can observe that the resonance energies become increasingly negative as the inter-dot distance grows, reflecting the stabilization of the quasi-bound states. The sensitivity of the energy of the resonances to these small variations in the potential, remains negligible and does not show any noticeable impact on the physics of ICD: The ICD decay rates obtained in time-dependent simulations with both MGPF and MCCPD exhibit a clear R^{-6} dependence, characteristic of long-range dipole-dipole coupling. These rates decrease by several orders of magnitude as the dots are separated, while the corresponding lifetimes increase accordingly up to a nanosecond regime.

Overall, the combination of electronic structure and dynamical results confirms that the MCCPD representation yields a stable, accurate, and reproducible description of ICD in semiconductor quantum dots. The method captures both the qualitative behavior and the quantitative trends with controlled accuracy, making it a reliable tool for future investigations of Coulomb-driven decay mechanisms in low dimensional nanostructures even with a higher-dimensional continuum.

I. DATA AVAILABILITY

All potentials, input files and operator files can be made available upon reasonable request.

II. ACKNOWLEDGMENTS

The project was initially funded by Volkswagen Foundation via the Freigeist Fellowship No. 89525 and completed within the activities in the QD4ICEC German-French project funded by an ANR-DFG grant with a subproject of A.B. (BA3770/5-1) and of D.P. (ANR-22-CE92-0071-02). The computing resources of Freie Universität Berlin (HPC cluster Curta[31]) were used.

[1] L. S. Cederbaum, J. Zobeley, and F. Tarantelli, "Giant intermolecular decay and fragmentation of clusters," *Physical Review Letters*, vol. 79, pp. 4778–4781, 12 1997.

[2] U. Hergenhahn, "Interatomic and intermolecular coulombic decay: The early years," *Journal of Electron Spectroscopy and Related Phenomena*, vol. 184, pp. 78–90, 4 2011.

[3] T. Jahnke, "Interatomic and intermolecular Coulombic decay: the coming of age story," *J. Phys. B: At. Mol. Opt. Phys.*, vol. 48, p. 082001, 2015. experiment theory.

[4] T. Jahnke, U. Hergenhahn, B. Winter, R. Dörner, U. Frühling, P. V. Demekhin, K. Gokhberg, L. S. Cederbaum, A. Ehresmann, A. Knie, and

A. Dreuw, "Interatomic and intermolecular coulombic decay," *Chemical Reviews*, vol. 120, pp. 11295–11369, 10 2020.

[5]A. Bande, K. Gokhberg, and L. S. Cederbaum, "Dynamics of interatomic coulombic decay in quantum dots," *Journal of Chemical Physics*, vol. 135, 2011.

[6]F. Weber, E. F. Aziz, and A. Bande, "Interdependence of icd rates in paired quantum dots on geometry," *Journal of Computational Chemistry*, vol. 38, pp. 2141–2150, 9 2017.

[7]J.-L. Schäfer, F. Langkabel, and A. Bande, "Three-electron dynamics of the interparticle coulombic decay in doubly excited clusters with one-dimensional continuum confinement," *Molecules*, vol. 27, p. 8713, 12 2022.

[8]S. Marando and A. Bande, "Inter-particle coulombic decay of highly excited resonance states: A study on competing relaxation mechanisms," *The Journal of Chemical Physics*, vol. 163, 7 2025.

[9]M. Beck, "The multiconfiguration time-dependent hartree (mctdh) method: a highly efficient algorithm for propagating wavepackets," *Physics Reports*, vol. 324, pp. 1–105, 1 2000.

[10]J. Broeckhove and L. Lathouwers, eds., *Time-Dependent Quantum Molecular Dynamics*, vol. 299. Springer US, 1992.

[11]J. C. Light and T. Carrington, *Discrete-Variable Representations and their Utilization*, pp. 263–310. 1 2000.

[12]F. Langkabel and A. Bande, "Three-electron dynamics of the interparticle Coulombic decay with two-dimensional continuum confinement," *Journal of Chemical Physics*, vol. 154, p. 054111, 2021. theory.

[13]A. Haller, D. Peláez, and A. Bande, "Inter-coulombic decay in laterally arranged quantum dots controlled by polarized lasers," *The Journal of Physical Chemistry C*, vol. 123, p. 14754, 2019.

[14]P. Dolbundalchok, D. Peláez, E. F. Aziz, and A. Bande, "Geometrical control of the interatomic coulombic decay process in quantum dots for infrared photodetectors," *Journal of Computational Chemistry*, vol. 37, pp. 2249–2259, 9 2016.

[15]A. Jäckle and H.-D. Meyer, "Product representation of potential energy surfaces," *Journal of Chemical Physics*, vol. 104, pp. 7974–7984, 1996.

[16]D. Peláez and H.-D. Meyer, "The multigrid potfit (mgpf) method: Grid representations of potentials for quantum dynamics of large systems," *The Journal of Chemical Physics*, vol. 138, 1 2013.

[17]D. Neuhasuer and M. Baer, "The time-dependent schrödinger equation: Application of absorbing boundary conditions," *The Journal of Chemical Physics*, vol. 90, pp. 4351–4355, 4 1989.

[18]D. Neuhauser, M. Baer, R. S. Judson, and D. J. Kouri, "The application of time-dependent wavepacket methods to reactive scattering," *Computer Physics Communications*, vol. 63, pp. 460–481, 2 1991.

[19]U. V. Riss and H. D. Meyer, "Calculation of resonance energies and widths using the complex absorbing potential method," *Journal of Physics B: Atomic, Molecular and Optical Physics*, vol. 26, pp. 4503–4535, 12 1993.

[20]R. Salvai, S. K. Das, F. M. Pont, S. Marando, D. Peláez, and A. Bande in preparation, 2026.

[21]A. Bande, F. M. Pont, P. Dolbundalchok, K. Gokhberg, and L. S. Cederbaum, "Electron dynamics of interatomic coulombic decay in quantum dots: Singlet initial state," *EPJ Web of Conferences*, vol. 41, p. 04031, 3 2013.

[22]M. Schröder, "Transforming high-dimensional potential energy surfaces into a canonical polyadic decomposition using monte carlo methods," *The Journal of Chemical Physics*, vol. 152, 1 2020.

[23]H.-D. Meyer, U. Manthe, and L. Cederbaum, "The multi-configurational time-dependent hartree approach," *Chemical Physics Letters*, vol. 165, pp. 73–78, 1 1990.

[24]H.-D. Meyer, F. Gatti, and G. A. Worth, *Multidimensional Quantum Dynamics*. Wiley, 4 2009.

[25]Y. Sajeev and N. Moiseyev, "Theory of autoionization and photoionization in two-electron spherical quantum dots," *Physical Review B*, vol. 78, p. 075316, 8 2008.

[26]NSM Archive, "Physical properties of semiconductors: Gaas." `http://matprop.ru/GaAs_basic`. Accessed: March 2026.

[27]H.-D. Meyer, F. Le Quéré, C. Léonard, and F. Gatti, "Calculation and selective population of vibrational levels with the multiconfiguration time-dependent hartree (mctdh) algorithm," *Chemical Physics*, vol. 329, pp. 179–192, 2006.

[28]R. Kosloff and H. Tal-Ezer, "A direct relaxation method for calculating eigenfunctions and eigenvalues of the schrödinger equation on a grid," *Chemical Physics Letters*, vol. 127, pp. 223–230, 1986.

[29]V. Averbukh and P. Kolorenč, "Collective interatomic decay of multiple vacancies in clusters," *Physical Review Letters*, vol. 103, p. 183001, 10 2009.

[30]A. I. Kuleff, K. Gokhberg, S. Kopelke, and L. S. Cederbaum, "Ultrafast interatomic electronic decay in multiply excited clusters," *Physical Review Letters*, vol. 105, p. 043004, 7 2010.

[31]L. Bennett, B. Melchers, and B. Proppe, "Curta: A general-purpose high-performance computer at zedat, freie universität berlin." http://dx.doi.org/10.17169/refubium-26754, 2020.